
STD-LLM: Understanding Both Spatial and Temporal Properties of Spatial-Temporal Data with LLMs

Yiheng Huang* Xiaowei Mao* Shengnan Guo Yubin Chen Youfang Lin Huaiyu Wan†
{huangyiheng,maoxiaowei,guoshn,chenyubin,yflin,hywan}@bjtu.edu.cn

Abstract

Spatial-temporal forecasting and imputation are important for real-world dynamic systems such as intelligent transportation, urban planning, and public health. Most existing methods are tailored for individual forecasting or imputation tasks but are not designed for both. Additionally, they are less effective for zero-shot and few-shot learning. While large language models (LLMs) have exhibited strong pattern recognition and reasoning abilities across various tasks, including few-shot and zero-shot learning, their development in understanding spatial-temporal data has been constrained by insufficient modeling of complex correlations such as the temporal correlations, spatial connectivity, non-pairwise and high-order spatial-temporal correlations within data. In this paper, we propose STD-LLM for understanding both spatial and temporal properties of Spatial-Temporal Data with LLMs, which is capable of implementing both spatial-temporal forecasting and imputation tasks. STD-LLM understands spatial-temporal correlations via explicitly designed spatial and temporal tokenizers as well as virtual nodes. Topology-aware node embeddings are designed for LLMs to comprehend and exploit the topology structure of data. Additionally, to capture the non-pairwise and higher-order correlations, we design a hypergraph learning module for LLMs, which can enhance the overall performance and improve efficiency. Extensive experiments demonstrate that STD-LLM exhibits strong performance and generalization capabilities across the forecasting and imputation tasks on various datasets. Moreover, STD-LLM achieves promising results on both few-shot and zero-shot learning tasks.

1 Introduction

Understanding both spatial and temporal properties of spatial-temporal data (e.g., the dependencies and changing patterns of data in spatial-temporal dimensions) is crucial for various real-world dynamic systems such as intelligent transportation [1], urban planning [2], and public health. In practice, spatial-temporal forecasting [3, 4] and imputation [5, 6] are the two most pivotal and common tasks relying on understanding the properties of spatial-temporal data. Specifically, precise spatial-temporal forecasting aids in effective traffic management and travel planning, and spatial-temporal imputation fills in missing data caused by unforeseen events during data collection and storage, enabling precise analysis of spatial-temporal patterns and supporting other dependent tasks. Although extensive studies have achieved satisfactory accuracy in spatial-temporal forecasting and imputation, they rely on extensive historical data for training. However, obtaining comprehensive datasets for all the studied regions is challenging due to the high cost of collecting and storing long-term data. Consequently, the zero-shot [7] and few-shot learning [8] capabilities are hindered for spatial-temporal forecasting methods across different regions. Moreover, existing methods are usually tailored to specific tasks and not designed for both forecasting and imputation. Each method requires

*These authors contribute equally to this work. † Corresponding authors.

domain expertise and task-specific designs, increasing costs and complicating the deployment of forecasting and imputation methods. To summarize, we need a method that possesses powerful zero-shot and few-shot learning capabilities and is versatile for both spatial-temporal forecasting and imputation tasks, making it practical and applicable in real-world scenarios.

We have noticed that pre-trained Large Language Models (LLMs) [9, 10] are widely recognized for strong performance in zero-shot and few-shot learning in unfamiliar scenarios for various natural language processing tasks. Additionally, they are applicable across a diverse range of tasks [11, 12]. However, due to the significant differences in modality between spatial-temporal and textual data used in the pre-training process of LLMs, it is challenging to fine-tune LLMs to comprehend spatial-temporal data. In addition, training a spatial-temporal LLM from scratch is non-trivial due to the limited availability of spatial-temporal data compared to textual data. To address this issue, researchers have attempted to adapt pre-trained LLMs for understanding spatial-temporal data by creating tokenizers designed for fine-tuning LLMs [13, 14]. However, these methods offer insufficient representation for spatial-temporal data. Thus, they are less effective for understanding both spatial and temporal properties of spatial-temporal data with LLMs. First, existing methods, such as [13, 14], design tokens along the spatial dimension but ignore the tokens obtained from the temporal dimension. Second, topological connectivity information inherent in spatial-temporal data is less explored for empowering zero-shot learning capabilities. Thirdly, existing methods focus on modeling pairwise relations of tokens in the spatial dimension. They are less effective in capturing non-pairwise and higher-order spatial-temporal correlations. On the other hand, existing LLM-based spatial-temporal forecasting methods primarily concentrate on forecasting tasks and overlook the task of imputation. This limitation restricts their versatility and efficiency for practical applications.

To solve the above limitations and challenges, we propose STD-LLM for understanding both spatial-temporal properties of Spatio-Temporal Data with LLMs. First, we create spatial-temporal embeddings for fully capturing temporal correlations and exploiting the topology structure of data along the spatial dimension. Second, we develop a spatial tokenizer and a temporal tokenizer to activate the ability of pre-trained LLM to understand spatial-temporal data from both the spatial and temporal dimensions while incorporating the topology structure of data. Lastly, we design a hypergraph learning module to capture non-pairwise and higher-order spatial-temporal correlations and reduce the computational cost, particularly in scenarios with large graph structures. Based on the explicitly designed tokenization and hypergraph learning equipped for fine-tuning the LLM, STD-LLM is not only versatile for spatial-temporal forecasting and imputation but also exhibits accurate few-shot and zero-shot learning capabilities on spatial-temporal data. In summary, our contributions can be summarized as follows:

- We propose STD-LLM for accurate spatial-temporal forecasting and imputation, as well as zero-shot and few-shot learning, by activating LLMs to understand both the spatial and temporal properties of ST data.
- We develop temporal tokenizers and spatial tokenizers to construct tokens from spatial and temporal perspectives to activate LLM to understand spatial-temporal data while incorporating the topology structure inherent in data.
- We design a hypergraph learning module to model the non-pairwise and higher-order spatial-temporal correlations in the spatial-temporal data. By incorporating the hypergraph learning module, we not only enhance the overall performance but also improve efficiency.

2 Related Work

Spatial-Temporal Data Forecasting. As a problem with a wide range of applications, there is a lot of work for this problem. Initial studies[15, 16] utilizing conventional time-series analysis techniques which based on basic statistical features of time series. In recent years, with the rapid development of deep learning, a large number of models that can effectively model spatial-temporal dependencies have emerged. Several studies [17] address temporal dynamics using RNNs and their derivatives. To deal with spatial dependency, the data can be divided into grids [18, 19, 20, 21], and then CNNs are utilized to capture spatial correlations. This approach is somewhat effective, but not all data can be partitioned into grid form. In order to achieve a more general and effective model, researchers introduced the graph convolution model[22, 23] thereby implementing spatial feature aggregation based on adjacency matrices [24, 25, 26, 27, 28, 3]. AGCRN[3] uses individual weights and biases

for each node during GCN feature transformations to learn patterns specific to each node, and to remove the constraints of a priori adjacency matrices while constructing dynamic graph networks, AGCRN also can learn adjacency matrices adaptively from data by node embedding. Models such as GMANZheng et al. [29], ASTGCN[30] and ASTGNN[4] utilize attention mechanisms to further deal with temporal and spatial correlations. PDFormer[31] devised a spatial self-attention module to model global semantic neighborhoods and geographically localized neighborhoods separately via graph masking, and proposed a delay-aware feature transformation module to explicitly model the temporal delay of propagation. The current work has a fairly good forecasting accuracy, but most of the models do not take into account the few-shot learning, zero-shot learning.

Spatial-Temporal Data Imputation. Initially, researchers used interpolation algorithms, KNN and other algorithms to accomplish the imputation of some simple scenes. In order to realize imputation in more complex scenes, successive works based on low-rank matrix completion[32, 33] and random forest[34] were proposed. LATC[35] effectively captures local and global trends in the data by combining low-rank matrix completion with an auto-regressive model. The development of deep learning has also contributed to the research on imputation. Brits[5] build an efficient self-supervised imputation model by capturing complex correlations between different features, time through bidirectional LSTM. E2GAN[36], GAIN[37] and other GAN[38] based models transform the imputation problem into a generative problem. In addition, some VAE[39] based work recovers missing values by modeling the distribution of the data in the hidden space and recovering the hidden state obtained by sampling from the distribution. Such as mTAN[40] obtains a representation of the data in the hidden space through the attention between the reference point and the incomplete sequence. Recently the powerful effect of Diffusion Model[41] in the field of image generation attracts a large number of researchers, and some imputation work based on Diffusion Model has also appeared. CSDI[42] is based on the Conditional Diffusion Model, which uses the observable as a conditional input, and learns the correlation between time and space through the attention mechanism. Compared to CSDI, PriSTI[6] adds conditional feature extraction module and graph neural network, which enhances the utilization of conditional information and the construction of geographic prior knowledge. Existing imputation models face the same problem as forecasting models, both need to reduce the need for training samples and enhance generalization capabilities.

Large Language Model. LLMs provide a powerful and unified framework for different tasks and have attracted a large number of researchers. There has been a significant amount of recent work validating the effectiveness of the LLM in other modalities. One Fits All(OFA)[12] demonstrated the feasibility of using large models for time series data through the experimental results of eight different temporal tasks, and put forward preliminary explanations. Articles such as Time-LLM[43] make more detailed modifications to LLM, using methods such as reprogramming, prompt pool, and contrast learning to align temporal and textual data. Models such as STLLM[14] and STGLLM[13] enhance LLM’s perception of spatial-temporal data by constructing tokens in the dimension of space, combined with the fine-tuning method of partial freezing. Existing spatial-temporal data large models have achieved certain results, confirming that LLM has the ability to handle spatial-temporal data. However, they underutilize spatial information and are difficult to accurately capture complex spatial dependencies, and there is much room for improvement.

3 Methodology

3.1 Problem Definition

Spatial-Temporal data. Considering spatial-temporal data with T time slices and N nodes, we represent it as $\mathcal{X} = \{\mathbf{X}_1, \mathbf{X}_2, \dots, \mathbf{X}_T\} \in \mathbb{R}^{T \times N \times C}$. Here, $\mathbf{X}_t = \{\mathbf{x}_{t,1}, \mathbf{x}_{t,2}, \dots, \mathbf{x}_{t,N}\} \in \mathbb{R}^{N \times C}$, where $\mathbf{x}_{t,n}$ represents the feature vector of node n at time slice t , and C is the number of features. We use a binary mask tensor $\mathcal{M} \in \{0, 1\}^{T \times N \times C}$ to denote the positions of missing values in \mathcal{X} , where $m_{t,n,c} = 0$ indicates that the data is missing, and $m_{t,n,c} = 1$ indicates that the data is observed. To more accurately capture spatial correlations, we use a directed graph $\mathcal{G} = (\mathcal{V}, \mathcal{E}, \mathbf{A})$ to describe the relationships between nodes. Here, \mathcal{V} represents the set of nodes in the data. \mathcal{E} is the set of edges that depict the spatial relationships such as geographical distance and adjacency between nodes. $\mathbf{A} \in \mathbb{R}^{N \times N}$ is the adjacency matrix of the graph \mathcal{G} .

Forecasting task. Given the historical spatial-temporal data with T time slices $\{\mathbf{X}_{t-T+1}, \dots, \mathbf{X}_{t-1}, \mathbf{X}_t\}$ and the corresponding graph structure, the objective is to learn a function f with parameters θ to

forecast future spatial-temporal data $\{\mathbf{X}_{t+1}, \dots, \mathbf{X}_{t+P-2}, \mathbf{X}_{t+P-1}\}$ for the next P time slices.

$$\{\mathbf{X}_{t+1}, \dots, \mathbf{X}_{t+P-2}, \mathbf{X}_{t+P-1}\} = f_{\theta}(\{\mathbf{X}_{t-T+1}, \dots, \mathbf{X}_{t-1}, \mathbf{X}_t\}, \mathcal{G}). \quad (1)$$

Imputation task. Given spatial-temporal data with T time slices $\{\tilde{\mathbf{X}}_{t-T+1}, \dots, \tilde{\mathbf{X}}_{t-1}, \tilde{\mathbf{X}}_t\}$ that contain missing values, the goal is to learn a function f with parameters θ to estimate missing values.

$$\{\mathbf{X}_{t-T+1}, \dots, \mathbf{X}_{t-1}, \mathbf{X}_t\} = f_{\theta}(\{\tilde{\mathbf{X}}_{t-T+1}, \dots, \tilde{\mathbf{X}}_{t-1}, \tilde{\mathbf{X}}_t\}, \mathcal{M}, \mathcal{G}). \quad (2)$$

3.2 Model Structure

As shown in Figure 1, our model focuses on accurate spatial-temporal forecasting and imputation via fine-tuning the LLM to understand the dependencies and evolving patterns in spatial-temporal data. To achieve this, we first develop spatial-temporal embedding to exploit the topology structure and periodicity of data. Based on this, we design temporal and spatial tokenizers to convert the spatial-temporal data into sequential tokens, enabling the LLM to learn the inherent spatial-temporal dependencies and evolving patterns of the data represented in the sequential token format. Lastly, we further incorporate a hypergraph learning module to effectively capture the non-pairwise and higher-order spatial-temporal correlations in data.

Spatial-Temporal Embedding. The spatial-temporal embedding consists of a time embedding and a topology-aware node embedding, which explores the static properties of data in both the spatial and temporal dimensions.

Time embedding: Two kinds of temporal information, i.e., time-of-day and day-of-week, are exploited for creating embedding dictionaries, $\mathbf{D}_t \in \mathbb{R}^{288 \times d_t}$ and $\mathbf{D}_w \in \mathbb{R}^{7 \times d_t}$ for time-of-day and day-of-week, where d_t is the dimension of the time embedding. By the looking-up and concatenation along with broadcast operations, we finally obtain the time embedding $\mathbf{E}_T \in \mathbb{R}^{T \times N \times 2d_t}$.

topology-aware node embedding: It is designed to activate LLM to understand the topology structure in spatial-temporal data and facilitate LLM’s universality in handling data with different numbers of nodes.

The proposed topology-aware node embedding is obtained based on the eigendecomposition of the graph Laplacian matrix. There are two reasons for this design. First, as a matrix representation of the graph, the graph Laplacian matrix encapsulates the important information (i.e., connectivity, degree, and eigenvalues) about the graph, helping the model perceive the static spatial properties of data. Second, the graph Laplacian matrix has mutually orthogonal eigenvectors, helping the model modeling the connectivity of nodes.

Specifically, we define the Laplacian matrix $\mathbf{L} = \mathbf{I} - \mathbf{D}^{\frac{1}{2}} \mathbf{A} \mathbf{D}^{\frac{1}{2}}$, where $\mathbf{D} = \sum_{j=1}^N \mathbf{A}_{i,j}$ is the degree matrix and \mathbf{I} is the identity matrix. The eigendecomposition of \mathbf{L} yields $\mathbf{L} = \mathbf{V} \mathbf{\Lambda} \mathbf{V}^{-1}$, with \mathbf{V} being the matrix of eigenvectors and $\mathbf{\Lambda}$ the diagonal matrix of eigenvalues. By selecting the eigenvectors corresponding to the top K largest eigenvalues, we obtain $\mathbf{V}' \in \mathbb{R}^{N \times K}$. After passing through a linear layer, we broadcast to obtain the topology-aware node embedding $\mathbf{E}_N \in \mathbb{R}^{T \times N \times d_n}$:

$$\begin{aligned} \mathbf{w}^* &= \text{argtop}_K(\text{diag}(\mathbf{\Lambda})), \\ \mathbf{V}' &= \mathbf{V}[:, \mathbf{w}^*], \quad \mathbf{E}_N = \mathbf{W}_{ne} \mathbf{V}' + \mathbf{b}_{ne}, \end{aligned} \quad (3)$$

where "diag" refers to the operation of extracting the diagonal elements of a matrix. $\mathbf{W}_{ne} \in \mathbb{R}^{K \times d_n}$ and $\mathbf{b}_{ne} \in \mathbb{R}^{d_n}$ represent the trainable parameters of the linear layers.

The node embedding obtained through the eigendecomposition of the Laplacian matrix not only assists the LLM in understanding the topology structure in the spatial-temporal data. Furthermore, since the trainable parameters are independent of the graph, we can easily transfer our model between different graph structures, which is key to our model’s ability to perform well in zero-shot learning.

Spatial Tokenizer.

The spatial tokenizer is designed to convert the spatial-temporal data into sequential tokens by aggregating the information along the spatial dimension. Specifically, each node’s feature vectors over P time slices are encoded into a spatial token, as shown in Figure 2. We further include the topology structure of nodes into the spatial token by incorporating our proposed topology-aware node

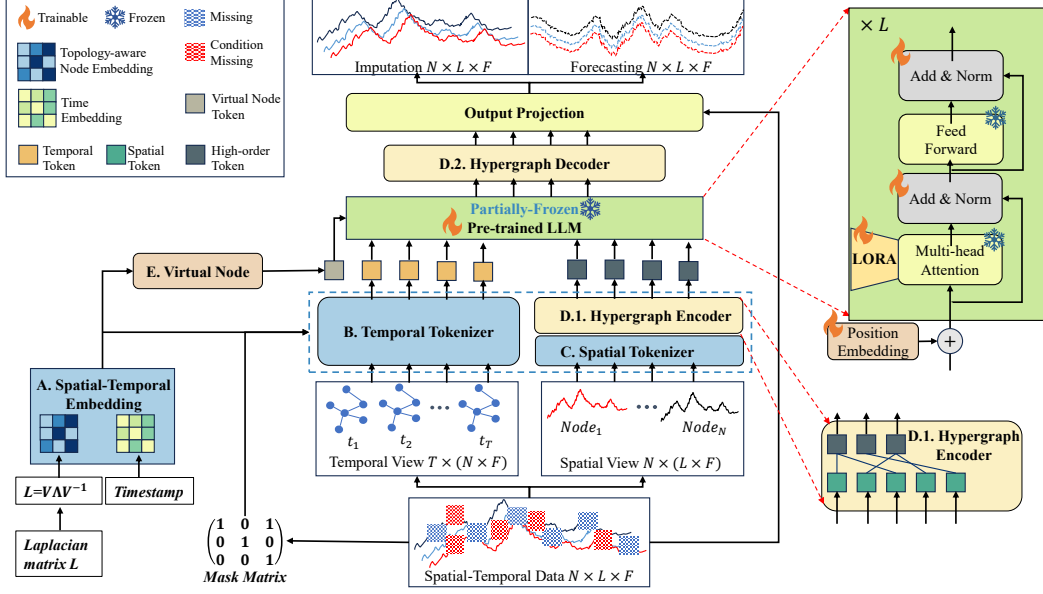


Figure 1: Model architecture. Condition missing refers to the additional generation of missing data on the training set for the purpose of training. Module **A** provides spatial-temporal embeddings for node and temporal information. The spatial-temporal tokenizers **B** and **C** construct temporal and spatial tokens from different perspectives. Module **D** builds higher-order spatial tokens based on the spatial tokens, which is the output of **C**. Module **E** models the impact of external systems.

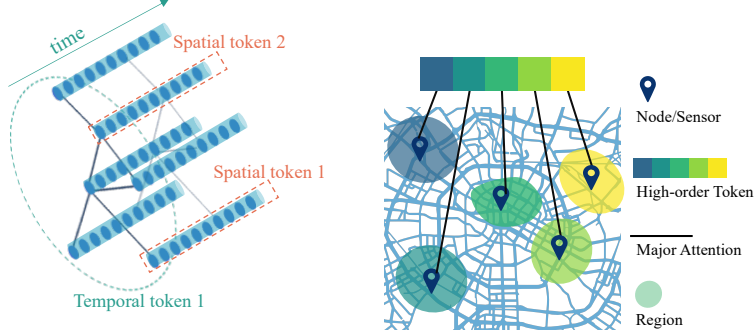


Figure 2: Spatial and Temporal tokens. Figure 3: Hypergraph Learning.

embedding. To keep the temporal information in the spatial token, We equip the spatial token with the time embedding, including $\mathbf{E}_t \in \mathbb{R}^{d_t}$ for the time-of-day, $\mathbf{E}_w \in \mathbb{R}^{d_w}$ for the day-of-week. It is worth noting that missing data are typically padding with the same value, which can result in high weights between missing positions during attention operation. This may lead to an inability to aggregate valid information, thereby affecting the accuracy of forecasting and imputation. Therefore, it is necessary to enhance the model's ability to perceive missing values. We generate mask tokens based on the mask matrix to enhance the model's ability to perceive missing values. The entire computational process in spatial tokenizer can be formalized as follows:

$$\begin{aligned}
 \mathbf{Z} &= \mathbf{W}_Z[\mathcal{X}||\mathbf{E}_T||\mathbf{E}_N||\mathcal{M}] + \mathbf{b}_Z, \\
 \mathbf{Z}_{mask} &= \mathbf{W}_{mask}\mathcal{M} + \mathbf{b}_{mask}, \\
 \mathbf{Z}_S &= \text{LayerNorm}(\mathbf{Z} + \mathbf{Z}_{mask}),
 \end{aligned} \tag{4}$$

where \mathbf{W}_* and \mathbf{b}_* denote the trainable parameters. $||$ denotes concatenation along the feature dimension. $\mathbf{Z} \in \mathbb{R}^{N \times d_{LLM}}$ represents preliminary spatial tokens. d_{LLM} is the token dimension of the LLM. $\mathbf{Z}_{mask} \in \mathbb{R}^{N \times d_{LLM}}$ indicates the mask tokens which contain the missing pattern of the data. $\mathbf{Z}_S \in \mathbb{R}^{N \times d_{LLM}}$ represents our target spatial tokens.

Temporal Tokenizer. The temporal tokenizer is designed to activate the LLM to understand spatial-temporal data by converting the spatial-temporal data into sequential tokens along the temporal dimension. We aim to encode the spatial-temporal data at each time slice into a token. Specifically, We first concatenate the spatial-temporal data, the time embedding, topology-aware node embedding, and the binary mask tensor, then aggregate various types of information through MLP to obtain the hidden representation $\mathbf{F} \in \mathbb{R}^{T \times N \times d_T}$. Subsequently, we utilize attention mechanism to aggregate the information of nodes in the hidden space, resulting in $\mathbf{H}_T \in \mathbb{R}^{T \times 1 \times d_T}$. In this process, we need to aggregate information across the spatial dimension while ensuring that the model can adapt to different graph structures. Therefore, using methods such as self-attention is not suitable. To address this, we learn reference points $\mathbf{Q}_l \in \mathbb{R}^{T \times 1 \times d_T}$ for each time step to aggregate information across the spatial dimension by interacting with nodes. The process is defined as follows:

$$\text{Attention}(\mathbf{Q}, \mathbf{K}, \mathbf{V}) = \text{Softmax}\left(\frac{\mathbf{Q}\mathbf{K}^T}{\sqrt{d_k}}\right)\mathbf{V}, \quad (5)$$

$$\begin{aligned} \mathbf{F} &= \text{MLP}((\mathbf{W}_F[\mathcal{X}||\mathcal{M}] + \mathbf{b}_F)||\mathbf{E}_T||\mathbf{E}_N), \\ \mathbf{H}_T &= \text{Attention}(\mathbf{Q}_l, \mathbf{F}, \mathbf{F}), \\ \mathbf{Z}_T &= \text{LayerNorm}(\mathbf{W}_T\mathbf{H}_T + \mathbf{b}_T), \end{aligned} \quad (6)$$

where \mathbf{W}_* and \mathbf{b}_* denote the trainable parameters. d_k is the feature dimension, which is used for normalizing the variance in the attention mechanism. The MLP consists of two layers of linear with a ReLU activation function in between. Within the attention operation, we compute the similarity between the reference node and the hidden representation of each node, and subsequently aggregate the hidden representations of the nodes based on these similarities to obtain \mathbf{H}_T . Finally, a linear layer followed by LayerNorm is applied to obtain the temporal tokens $\mathbf{Z}_T \in \mathbb{R}^{T \times d_{LLM}}$.

Hypergraph Learning We can capture the pair-wise correlation using spatial tokens aggregated by nodes, but it is difficult to capture important non-pairwise and higher-order spatial-temporal dependencies. To capture higher-order spatial-temporal correlations, we project node-level data into a region-level. For spatial-temporal data, the region is an appropriate choice, as the influencing factors, such as human activities and weather geological changes, exhibit distinct regional characteristics. Therefore, we design an autoencoder module to learn the mapping relationships between nodes and regions. The encoder, hypergraph encode, projects spatial tokens into higher-order region-level tokens. The decoder, hypergraph decode, is responsible for decoding the regional latent vectors back into node-level latent vectors. A simple implementation is to construct the encoder and decoder based on prior knowledge, but this approach overlooks the dynamics of the mapping relationships and cannot be easily transferred between different graph structures. Thus, we opted for attention mechanism-based encoders and decoders to dynamically learn these mapping relationships from the data. The process of hypergraph encode constructing region-level tokens $\mathbf{Z}_H \in \mathbb{R}^{M \times d_{LLM}}$ (M represents the number of regions) from spatial tokens is as follows:

$$\begin{aligned} \mathbf{H}_N &= \mathbf{W}_N\mathbf{Z}_S + \mathbf{b}_N, \\ \mathbf{Z}_H &= \text{LayerNorm}(\mathbf{W}_H\text{Attention}(\mathbf{H}_l, \mathbf{H}_N, \mathbf{H}_N) + \mathbf{b}_H), \end{aligned} \quad (7)$$

where $\mathbf{H}_N \in \mathbb{R}^{N \times d_H}$ represents the lower-dimensional representation of \mathbf{Z}_S after passing through a linear layer. d_H is the hidden dimension. $\mathbf{H}_l \in \mathbb{R}^{M \times d_H}$ is a set of learnable parameters that extract regional-level representations.

After \mathbf{Z}_H is processed by the LLM to obtain its hidden representation $\mathcal{Z}_H \in \mathbb{R}^{M \times d_{LLM}}$, it is necessary to map the regional-level hidden representation back to the node level by hypergraph decode to perform subsequent tasks:

$$\begin{aligned} \mathbf{H}_R &= \mathbf{W}_{hidden}\mathcal{Z}_H + \mathbf{b}_{hidden}, \\ \mathcal{Z}_N &= \text{LayerNorm}(\mathbf{W}_R\text{Attention}(\mathbf{H}_N, \mathbf{H}_l, \mathbf{H}_R) + \mathbf{b}_R). \end{aligned} \quad (8)$$

In this recovery process, $\mathbf{H}_R \in \mathbb{R}^{M \times d_H}$ is the lower-dimensional representation of \mathcal{Z}_H . $\mathcal{Z}_N \in \mathbb{R}^{N \times d_{LLM}}$ refers to the recovered node-level hidden representation from the LLM.

To ensure that the regional-level tokens constructed by the Hypergraph module can preserve the connectivity between nodes, a constraint loss function is designed. Furthermore, to prevent nodes from being ignored during the attention mechanism if their weights are too low, we have also added

regularization term for the constraint loss. Assuming $S \in \mathbb{R}^{M \times N}$ represents the attention weights between each regional-level token and node token, the constraint loss \mathcal{L}_C can be expressed as:

$$\mathcal{L}_C = - \sum_{m=1}^M \sum_{i,j,(i \neq j)} S_{m,i} S_{m,j} A_{i,j} + \underbrace{\log \pi(\text{Softmax}(\sum_{m=1}^M S_{m,:}) | \alpha)}_{\text{regularization term}}. \quad (9)$$

Here, π is the Dirichlet distribution. α is the parameter of the Dirichlet distribution. $S_{m,:}$ denotes the vector of attention weights for the m -th regional token across all node tokens, and its sum is fixed, which can encourage the regional tokens to aggregate information from node tokens that are connected in the graph. A thorough explanation is available in the Appendix E.

Virtual Node. The spatial-temporal data we encounter often does not exist within an isolated and closed system, where external changes can have a substantial impact. For example, in traffic flow forecasting tasks, the entry and exit of external vehicles can significantly affect it. Thus, it is necessary to model the impact of external systems. For spatial-temporal data, the impact is primarily manifested in the interplay between time and space. So we utilize an attention mechanism between \mathbf{E}_T and \mathbf{E}_N to obtain T tokens that represent the impact of external systems. Additionally, a learnable token is introduced to model some inherent characteristics of the external system that are independent of time. By combining these two components, the final virtual node $\mathbf{Z}_E \in \mathbb{R}^{(T+1) \times d_{LLM}}$ is derived to represent the influence of external changes.

Versatility for Spatial-Temporal Forecasting and Imputation Tasks. The main differences between forecasting and imputation lie in missing values and context. Forecasting tasks typically have few missing values and can only forecast based on historical values. Imputation tasks, on the other hand, have more missing data and can impute based on both historical and future values. In the Equation 4, we have already enhanced the model’s perception of missing values through the mask tokens. For the differences in context, the generalization ability of LLM can also effectively address it. Therefore, STD-LLM possess the capability to unify these two tasks. Switching between forecasting and imputation tasks can be achieved by modifying the target labels in the training dataset. Additionally, forecasting can be viewed as imputation of future missing values, thus unifying the two tasks. The model’s processing flow can be summarized as follows:

$$\begin{aligned} \mathbf{Z} &= \text{LLM}([\mathbf{Z}_E | \mathbf{Z}_T | \mathbf{Z}_H]), \\ \mathbf{Z}_H &= \mathbf{Z}[-M :, :], \quad \mathbf{Z}_N \leftarrow \mathbf{Z}_H, \\ \mathbf{Y} &= \text{MLP}([\mathbf{W}_Y \mathbf{Z}_N + \mathbf{b}_Y | \mathbf{X}]), \end{aligned} \quad (10)$$

where, $\mathbf{Y} \in \mathbb{R}^{N \times (P \times C)}$ is the forecasting or imputation result, P is the number of target time steps. \mathbf{X} is reshaped to $\mathbf{X} \in \mathbb{R}^{N \times (T \times C)}$ for processing convenience. \mathbf{W}_* and \mathbf{b}_* denote the trainable parameters of the linear layers. The "LLM" in equation refers to the main body of the pre-trained LLM. The last line of the formula denote to the decoding step of the Decoder.

4 Experiments

4.1 Datasets

The experiments conducted on four publicly available real-world traffic datasets (PEMS03, PEMS04, PEMS07, PEMS08) to validate the effectiveness and generalization capability of STD-LLM. PEMS means Caltrans Performance Measurement System (PeMS)[44], which is a system that collects data from the California highway network. The details of the four datasets are provided in Appendix C.2.

To test the model’s imputation capabilities under different scenarios, we generated missing data for testing using two type of missing C.3: RM (random missing), CM (spatial-temporal continuity missing) and two rates of missing - 30%, 70% on the dataset. Additionally, following the self-supervised training approach of CSDI[42], we generated condition missing for training. Condition missing refers to the artificially created missing data, used to generate training samples.

4.2 Experimental Settings

We follow the approach of ASTGCN[30] by partitioning the dataset into training set, validation set, and testing set with a ratio of 6: 2: 2, and employ a sliding window of size 12 to construct samples that forecast the next 12 steps based on the historical 12 steps.

To comprehensively compare the performance of models, we selected five representative baselines for the forecasting task, including Long Short-Term Memory network(LSTM)[45], ASTGCN[30], AGCRN[3], ASTGNN[4], PDFormer[31], OFA[12], and STGLLM[13]. For the imputation task, we also chose four well-known baselines, which are Brits[5], E2GAN[36], mTAN[40], and PriSTI[6].

The experiments were conducted on an Ubuntu 23.04 operating system with a PyTorch version of 2.1.2. The AdaW optimizer was utilized to optimize the model. The learning rate was set to 1×10^{-3} . The training epoch is 500 with an early stopping mechanism based on a patience of 50 epochs. The loss function used was L1 loss. We use GPT-2[46] as the pre-trained LLM and utilized only its initial three layers. STD-LLM employs the hyperparameters identified through tuning on the PEMS08 validation set for all datasets, ensuring the model’s generalization capability across different datasets. The detail of experiments settings are depicted in Appendix C.

4.3 Overall Performance

We measure the model’s performance using three widely used metrics for regression tasks: Mean Absolute Error (MAE), Root Mean Square Error (RMSE), and Mean Absolute Percentage Error (MAPE). Table 1 shows the forecasting performances comparison between our proposed STD-LLM and baselines. Bold indicates the best results, while underline denotes the second-best results. From Table 1, we can observe that: 1) The accuracy of the time series models such as LSTM and OFA is not good enough compared to methods that can handle spatial-temporal correlations in data. This indicates that relying solely on temporal correlation is insufficient to achieve high-precision forecasting; 2) The results obtained from OFA and STGLLM suggest that it is challenging for LLM to capture key information such as topological structure and higher-order spatiotemporal dependencies relying solely on its capabilities. This implies that it is necessary for us to design spatial and temporal tokenizers, topology-aware node embeddings, and hypergraph learning module to assist the LLM in understanding spatial and temporal properties. 3) Our proposed method achieve the best or second-best results on the PEMS04, PEMS07, and PEMS08 datasets.

Table 2 presents the imputation performances comparison between our proposed STD-LLM and baselines. Based on the comparison, we can observe that: 1) Our method achieves state-of-the-art performance in most scenarios. Although it underperforms in the CM 30%, it still attains the second-best results; 2) As the rate of missing data increases, the performance advantage of STD-LLM becomes more pronounced. This suggests that our method can more accurately capture higher-order correlations and other critical information from a small amount of data, demonstrating the capability to handle highly incomplete data; 3) STD-LLM exhibits a significant advantage in the RM case, particularly with a substantial improvement over other baseline models in the RM 70% case.

In summary, the experimental results demonstrate that STD-LLM has strong performance and can achieve high accuracy in both forecasting and imputation tasks.

Table 1: Forecasting performance.

Model	PEMS03			PEMS04			PEMS07			PEMS08		
	MAE	RMSE	MAPE(%)	MAE	RMSE	MAPE(%)	MAE	RMSE	MAPE(%)	MAE	RMSE	MAPE(%)
LSTM	20.62	33.54	28.94	26.81	40.74	22.33	29.71	45.32	14.14	22.19	33.59	18.74
ASTGCN	17.85	29.88	17.65	22.42	34.75	15.87	25.98	39.65	11.84	18.86	28.55	12.50
AGCRN	15.98	28.25	<u>15.23</u>	19.83	32.26	12.97	22.37	36.55	9.12	15.95	25.22	10.09
ASTGNN	<u>14.78</u>	<u>25.00</u>	14.79	18.60	30.91	12.36	20.62	34.00	8.86	15.00	24.70	9.50
PDFormer	14.74	25.59	15.35	<u>18.31</u>	29.97	<u>12.10</u>	<u>19.83</u>	32.87	<u>8.53</u>	13.58	<u>23.51</u>	<u>9.05</u>
OFA	20.96	33.43	19.11	27.37	42.99	17.97	30.53	47.51	12.98	21.89	34.63	13.30
STGLLM	15.26	24.11	15.73	20.00	32.11	13.69	21.98	35.02	9.72	15.53	24.74	10.15
STD-LLM (ours)	14.89	25.38	15.45	18.31	<u>30.32</u>	11.96	19.71	<u>32.99</u>	8.32	<u>13.85</u>	23.39	9.04

Table 2: Imputation performance on PEMS08. RM means the random missing. CM means the spatial-temporal continuity missing.

Model	RM 30%			RM 70%			CM 30%			CM 70%		
	MAE	RMSE	MAPE(%)	MAE	RMSE	MAPE(%)	MAE	RMSE	MAPE(%)	MAE	RMSE	MAPE(%)
BRITS	21.28	29.78	7.57	29.56	41.52	10.79	33.65	46.75	11.97	38.33	53.60	13.90
E2GAN	23.75	37.38	15.35	27.55	41.99	17.52	25.66	40.55	16.44	31.58	50.24	19.17
mTAN	20.29	32.62	12.71	<u>21.23</u>	<u>33.98</u>	12.89	24.50	40.23	15.07	31.42	49.10	18.96
PriSTI	<u>14.67</u>	<u>23.17</u>	9.55	25.54	36	16.73	17.8	34.67	10.71	<u>22.93</u>	<u>40.9</u>	14.43
STD-LLM (ours)	12.14	19.44	<u>8.06</u>	14.38	22.92	9.46	<u>19.36</u>	<u>34.53</u>	12.30	22.18	39.26	13.56

Table 3: Few-shot performance.

Ratio	PEMS04			PEMS08		
	MAE	RMSE	MAPE(%)	MAE	RMSE	MAPE(%)
5%	26.37	40.98	18.80	20.71	32.22	14.51
10%	24.15	37.91	16.57	19.60	31.09	12.85
20%	21.43	34.83	14.17	16.88	27.76	10.84

Table 4: Zero-shot performance.

	MAE	RMSE	MAPE(%)
PEMS04→PEMS08	25.95	39.60	21.74
PEMS08→PEMS04	29.29	46.01	22.46
PEMS07→PEMS03	23.58	35.50	38.27
PEMS03→PEMS07	33.79	51.63	18.73

4.4 Few-shot and Zero-shot Performance

To extensively evaluate the performance of LLMs on spatial-temporal tasks, we conduct few-shot and zero-shot experiments. The few-shot experiments evaluate the forecasting performance of STD-LLM on the PEMS04 and PEMS08 datasets using only the first 5%, 10%, and 20% of the training samples, with results summarized in Table 3. The zero-shot experiments evaluate the forecasting performance of the pre-trained model when applied to other datasets, with the results compiled in Table 4.

From Table 3, it can be observed that we only require 5% of the training samples to achieve performance comparable to that of LSTM trained on the full dataset. When the training samples are increased to 20%, the performance surpasses that of ASTGCN. This indicates that STD-LLM has excellent few-shot learning capabilities, which supports its application in scenarios where data is scarce. The results in Table 4 demonstrate that STD-LLM can exhibit acceptable performance when directly transferred to datasets with different temporal scopes and graph structures from the training set, without undergoing any training. Further experiments are presented in the Appendix F.

4.5 Ablation Study

Table 5: Ablation study.

Method	PEMS04			PEMS08			PEMS08 RM 70%			PEMS08 CM 70%		
	MAE	RMSE	MAPE(%)	MAE	RMSE	MAPE(%)	MAE	RMSE	MAPE(%)	MAE	RMSE	MAPE(%)
w/o Temporal Token	18.57	30.61	12.26	13.92	23.47	9.11	14.81	23.40	10.11	24.71	41.24	17.02
w/o Virtual Node	18.73	30.86	12.47	14.10	23.76	9.23	14.67	23.35	9.71	23.18	40.01	14.71
w/o Hypergraph	18.54	30.73	12.11	14.31	24.18	9.21	14.59	23.15	9.88	25.64	42.65	17.18
w/o LLM	18.96	30.88	12.82	14.25	23.47	9.36	21.66	36.60	21.12	104.30	133.72	197.80
STD-LLM	18.31	30.32	11.96	13.85	23.39	9.04	14.38	22.92	9.46	22.18	39.26	13.56

We implement ablation study to evaluate the effectiveness of each component. The ablation experiments compared our proposed model with the following variants: 1) w/o Temporal Token, removing the temporal tokens in Equation 6; 2) w/o Virtual Node, removing the virtual node; 3) w/o Hypergraph, removing the Hypergraph Learning module in Equation 7; 4) w/o LLM, replacing the LLM with a transformer encoder of the same layer and hidden dimension.

We summarize the results of the ablation study in Table 5. Based on the results, we can identify the following: 1) Temporal Token and Virtual Node can enhance the model’s forecasting and imputation performance with a relatively small computational cost. 2) The hypergraph module not only reduces the number of tokens, thereby increasing efficiency, but also significantly boosts the model’s performance. 3) The universal pattern recognition capabilities embodied in the pre-trained parameters of the LLM are useful for both spatiotemporal forecasting and imputation. Thus, LLM indeed play a substantial role in spatial-temporal forecasting and imputation, especially in scenarios with complex spatial-temporal dependencies, like the imputation task on PEMS08 CM 70%.

5 Conclusion

In this paper, we propose STD-LLM, a unified framework for spatial-temporal forecasting and imputation based on LLMs. Through our explicitly designed spatial and temporal tokenizers, STD-LLM can effectively understand both spatial and temporal properties of spatial-temporal data. To enhance the LLM’s understanding and utilization of the topology structure in spatial-temporal data, we have designed topology-aware node embeddings. Considering the impact of external systems, we have also introduced virtual nodes. In addition, we design a hypergraph learning module to enable the LLM to capture the non-pairwise and higher-order correlations by constructing region-level tokens. Extensive experiments demonstrate that STD-LLM exhibits strong generalization capabilities while maintaining competitive performance. Our work suggests that constructing a unified pre-trained large spatial-temporal model based on LLMs is a promising direction.

References

- [1] AiLing Ding, XiangMo Zhao, and LiCheng Jiao. Traffic flow time series prediction based on statistics learning theory. In *Proceedings. The IEEE 5th International Conference on Intelligent Transportation Systems*, pages 727–730. IEEE, 2002.
- [2] Qing Song, Dewei Li, and Xiaolei Li. Traffic prediction based route planning in urban road networks. In *2017 Chinese Automation Congress (CAC)*, pages 5854–5858. IEEE, 2017.
- [3] Lei Bai, Lina Yao, Can Li, Xianzhi Wang, and Can Wang. Adaptive graph convolutional recurrent network for traffic forecasting. *Advances in neural information processing systems*, 33:17804–17815, 2020.
- [4] Shengnan Guo, Youfang Lin, Huaiyu Wan, Xiucheng Li, and Gao Cong. Learning dynamics and heterogeneity of spatial-temporal graph data for traffic forecasting. *IEEE Transactions on Knowledge and Data Engineering*, 34(11):5415–5428, 2021.
- [5] Wei Cao, Dong Wang, Jian Li, Hao Zhou, Lei Li, and Yitan Li. Brits: Bidirectional recurrent imputation for time series. *Advances in neural information processing systems*, 31, 2018.
- [6] Mingzhe Liu, Han Huang, Hao Feng, Leilei Sun, Bowen Du, and Yanjie Fu. Pristi: A conditional diffusion framework for spatiotemporal imputation. *2023 IEEE 39th International Conference on Data Engineering (ICDE)*, pages 1927–1939, 2023. URL <https://api.semanticscholar.org/CorpusID:257038892>.
- [7] Wei Wang, Vincent W Zheng, Han Yu, and Chunyan Miao. A survey of zero-shot learning: Settings, methods, and applications. *ACM Transactions on Intelligent Systems and Technology (TIST)*, 10(2):1–37, 2019.
- [8] Yaqing Wang, Quanming Yao, James T Kwok, and Lionel M Ni. Generalizing from a few examples: A survey on few-shot learning. *ACM computing surveys (csur)*, 53(3):1–34, 2020.
- [9] Tom Brown, Benjamin Mann, Nick Ryder, Melanie Subbiah, Jared D Kaplan, Prafulla Dhariwal, Arvind Neelakantan, Pranav Shyam, Girish Sastry, Amanda Askell, et al. Language models are few-shot learners. *Advances in neural information processing systems*, 33:1877–1901, 2020.
- [10] Yupeng Chang, Xu Wang, Jindong Wang, Yuan Wu, Linyi Yang, Kaijie Zhu, Hao Chen, Xiaoyuan Yi, Cunxiang Wang, Yidong Wang, et al. A survey on evaluation of large language models. *ACM Transactions on Intelligent Systems and Technology*, 15(3):1–45, 2024.
- [11] Yingqiang Ge, Wenyue Hua, Kai Mei, Juntao Tan, Shuyuan Xu, Zelong Li, Yongfeng Zhang, et al. Openagi: When llm meets domain experts. *Advances in Neural Information Processing Systems*, 36, 2024.
- [12] Tian Zhou, Peisong Niu, Liang Sun, Rong Jin, et al. One fits all: Power general time series analysis by pretrained lm. *Advances in neural information processing systems*, 36, 2024.
- [13] Lei Liu, Shuo Yu, Runze Wang, Zhenxun Ma, and Yanming Shen. How can large language models understand spatial-temporal data? *arXiv preprint arXiv:2401.14192*, 2024.
- [14] Chenxi Liu, Sun Yang, Qianxiong Xu, Zhishuai Li, Cheng Long, Ziyue Li, and Rui Zhao. Spatial-temporal large language model for traffic prediction. *arXiv preprint arXiv:2401.10134*, 2024.
- [15] Eric Zivot and Jiahui Wang. Vector autoregressive models for multivariate time series. *Modeling financial time series with S-PLUS®*, pages 385–429, 2006.
- [16] Billy M Williams and Lester A Hoel. Modeling and forecasting vehicular traffic flow as a seasonal arima process: Theoretical basis and empirical results. *Journal of transportation engineering*, 129(6):664–672, 2003.
- [17] Xingjian Shi, Zhourong Chen, Hao Wang, Dit-Yan Yeung, Wai-Kin Wong, and Wang-chun Woo. Convolutional lstm network: A machine learning approach for precipitation nowcasting. *Advances in neural information processing systems*, 28, 2015.

- [18] Ziqian Lin, Jie Feng, Ziyang Lu, Yong Li, and Depeng Jin. Deepstn+: Context-aware spatial-temporal neural network for crowd flow prediction in metropolis. In *Proceedings of the AAAI conference on artificial intelligence*, volume 33, pages 1020–1027, 2019.
- [19] Ali Zonoozi, Jung-jae Kim, Xiao-Li Li, and Gao Cong. Periodic-crn: A convolutional recurrent model for crowd density prediction with recurring periodic patterns. In *IJCAI*, volume 18, pages 3732–3738, 2018.
- [20] Junbo Zhang, Yu Zheng, and Dekang Qi. Deep spatio-temporal residual networks for citywide crowd flows prediction. In *Proceedings of the AAAI conference on artificial intelligence*, volume 31, 2017.
- [21] Huaxiu Yao, Fei Wu, Jintao Ke, Xianfeng Tang, Yitian Jia, Siyu Lu, Pinghua Gong, Jieping Ye, and Zhenhui Li. Deep multi-view spatial-temporal network for taxi demand prediction. In *Proceedings of the AAAI conference on artificial intelligence*, volume 32, 2018.
- [22] Thomas N Kipf and Max Welling. Semi-supervised classification with graph convolutional networks. *arXiv preprint arXiv:1609.02907*, 2016.
- [23] Michaël Defferrard, Xavier Bresson, and Pierre Vandergheynst. Convolutional neural networks on graphs with fast localized spectral filtering. *Advances in neural information processing systems*, 29, 2016.
- [24] Yaguang Li, Rose Yu, Cyrus Shahabi, and Yan Liu. Diffusion convolutional recurrent neural network: Data-driven traffic forecasting. In *International Conference on Learning Representations*, 2018.
- [25] Lei Bai, Lina Yao, Salil S Kanhere, Xianzhi Wang, and Quan Z Sheng. Stg2seq: spatial-temporal graph to sequence model for multi-step passenger demand forecasting. In *Proceedings of the 28th International Joint Conference on Artificial Intelligence*, pages 1981–1987, 2019.
- [26] Haoyu Han, Mengdi Zhang, Min Hou, Fuzheng Zhang, Zhongyuan Wang, Enhong Chen, Hongwei Wang, Jianhui Ma, and Qi Liu. Stgcn: a spatial-temporal aware graph learning method for poi recommendation. In *2020 IEEE International Conference on Data Mining (ICDM)*, pages 1052–1057. IEEE, 2020.
- [27] Zonghan Wu, Shirui Pan, Guodong Long, Jing Jiang, and Chengqi Zhang. Graph wavenet for deep spatial-temporal graph modeling. *arXiv preprint arXiv:1906.00121*, 2019.
- [28] Chao Song, Youfang Lin, Shengnan Guo, and Huaiyu Wan. Spatial-temporal synchronous graph convolutional networks: A new framework for spatial-temporal network data forecasting. In *Proceedings of the AAAI conference on artificial intelligence*, volume 34, pages 914–921, 2020.
- [29] Chuanpan Zheng, Xiaoliang Fan, Cheng Wang, and Jianzhong Qi. Gman: A graph multi-attention network for traffic prediction. In *Proceedings of the AAAI conference on artificial intelligence*, volume 34, pages 1234–1241, 2020.
- [30] Shengnan Guo, Youfang Lin, Ning Feng, Chao Song, and Huaiyu Wan. Attention based spatial-temporal graph convolutional networks for traffic flow forecasting. In *Proceedings of the AAAI conference on artificial intelligence*, volume 33, pages 922–929, 2019.
- [31] Jiawei Jiang, Chengkai Han, Wayne Xin Zhao, and Jingyuan Wang. Pdformer: Propagation delay-aware dynamic long-range transformer for traffic flow prediction. In *Proceedings of the AAAI conference on artificial intelligence*, volume 37, pages 4365–4373, 2023.
- [32] Rahul Mazumder, Trevor Hastie, and Robert Tibshirani. Spectral regularization algorithms for learning large incomplete matrices. *The Journal of Machine Learning Research*, 11:2287–2322, 2010.
- [33] Hsiang-Fu Yu, Nikhil Rao, and Inderjit S Dhillon. Temporal regularized matrix factorization for high-dimensional time series prediction. *Advances in neural information processing systems*, 29, 2016.

- [34] Daniel J Stekhoven and Peter Bühlmann. Missforest—non-parametric missing value imputation for mixed-type data. *Bioinformatics*, 28(1):112–118, 2012.
- [35] Xinyu Chen, Mengying Lei, Nicolas Saunier, and Lijun Sun. Low-rank autoregressive tensor completion for spatiotemporal traffic data imputation. *IEEE Transactions on Intelligent Transportation Systems*, 23(8):12301–12310, 2021.
- [36] Yonghong Luo, Ying Zhang, Xiangrui Cai, and Xiaojie Yuan. E2gan: End-to-end generative adversarial network for multivariate time series imputation. In *Proceedings of the 28th international joint conference on artificial intelligence*, pages 3094–3100. AAAI Press Palo Alto, CA, USA, 2019.
- [37] Jinsung Yoon, James Jordon, and Mihaela Schaar. Gain: Missing data imputation using generative adversarial nets. In *International conference on machine learning*, pages 5689–5698. PMLR, 2018.
- [38] Ian Goodfellow, Jean Pouget-Abadie, Mehdi Mirza, Bing Xu, David Warde-Farley, Sherjil Ozair, Aaron Courville, and Yoshua Bengio. Generative adversarial networks. *Communications of the ACM*, 63(11):139–144, 2020.
- [39] Diederik P Kingma and Max Welling. Auto-encoding variational bayes. *stat*, 1050:1, 2014.
- [40] Satya Narayan Shukla and Benjamin M Marlin. Multi-time attention networks for irregularly sampled time series. *arXiv preprint arXiv:2101.10318*, 2021.
- [41] Jonathan Ho, Ajay Jain, and Pieter Abbeel. Denoising diffusion probabilistic models. *Advances in neural information processing systems*, 33:6840–6851, 2020.
- [42] Yusuke Tashiro, Jiaming Song, Yang Song, and Stefano Ermon. Csd: Conditional score-based diffusion models for probabilistic time series imputation. *Advances in Neural Information Processing Systems*, 34:24804–24816, 2021.
- [43] Ming Jin, Shiyu Wang, Lintao Ma, Zhixuan Chu, James Y Zhang, Xiaoming Shi, Pin-Yu Chen, Yuxuan Liang, Yuan-Fang Li, Shirui Pan, et al. Time-llm: Time series forecasting by reprogramming large language models. *arXiv preprint arXiv:2310.01728*, 2023.
- [44] Chao Chen, Karl Petty, Alexander Skabardonis, Pravin Varaiya, and Zhanfeng Jia. Freeway performance measurement system: mining loop detector data. *Transportation research record*, 1748(1):96–102, 2001.
- [45] Sepp Hochreiter and Jürgen Schmidhuber. Long short-term memory. *Neural computation*, 9(8): 1735–1780, 1997.
- [46] Alec Radford, Jeffrey Wu, Rewon Child, David Luan, Dario Amodei, Ilya Sutskever, et al. Language models are unsupervised multitask learners. *OpenAI blog*, 1(8):9, 2019.

A Limitations

Due to computational limitations, this paper did not further test whether LLM could yield better results. In theory, the recently emerged LLMs with 7 billion, 30 billion, or even more parameters should possess stronger capabilities for processing spatial-temporal data. Additionally, although this paper proposed a unified pre-training framework, we lack sufficient data to test whether the model, after being trained on a large-scale spatial-temporal dataset, would exhibit emergent phenomena similar to those of LLMs, leading to a substantial improvement in performance. These are some of the limitations of our research presented in this paper, and we hope that future work will be supported by adequate computational power and data to further explore these possibilities.

B Broader Impacts

Our proposed model can demonstrate relatively accurate spatial-temporal forecasting and imputation capabilities with only a small number of training samples or even without samples, which implies that our model can support a broader range of deployment and applications compared to other models. Moreover, the fast inference speed indicates that our model can sustain real-time interactive applications. Based on this, our work can provide rapid-response spatial-temporal forecasting services to a wider area, such as offering traffic dispatch decision support and travel route planning through accurate and swift traffic flow forecasting for different regions, thereby enhancing the efficiency of societal operations. However, a potential negative impact of this work is that inaccurate forecasting could lead to erroneous decision-making, resulting in adverse social consequences.

C Experimental Details

C.1 Baselines

To compare model performance, we selected 7 forecasting models and 4 imputation models as baselines. Detailed introductions to the baselines are as follows:

- LSTM: A special type of RNN (Recurrent Neural Network) that mitigates the vanishing and exploding gradient problems by incorporating memory cells and forget gates, enabling the processing of long-term dependencies in sequences.
- ASTGCN: A traffic forecasting model based on attention and convolutional networks. It captures the dynamic correlations of data through spatial-temporal attention and combines spatial-temporal graph convolutions to capture temporal features and spatial features.
- AGCRN: An adaptive graph convolutional neural network for traffic forecasting. It optimizes the conventional GCN (Graph Convolutional Network) by proposing a dynamic graph convolution algorithm that learns adaptively from the data. It learns transformation matrices for each node separately to better handle different spatial-temporal patterns of nodes. By integrating the dynamic graph convolution with GRU (Gated Recurrent Unit), it efficiently processes spatial-temporal data.
- ASTGNN: An autoregressive forecasting model based on spatial-temporal attention and dynamic graph convolution. It improves the traditional multi-head attention module by introducing 1D convolution to process hidden local trend variations in the data. It also optimizes the conventional GCN by modeling spatial heterogeneity through additional embedding vectors.
- PDFormer: An attention-based traffic forecasting model. It fully considers the shortcomings of conventional GNN (Graph Neural Network) models in handling dynamic spatial-temporal dependencies, long-range dependencies, and information propagation delays in traffic systems. By combining geographical distance and traffic similarity to generate semantic and geographical neighbors, it enables spatial-temporal attention to handle both short-range and long-range dynamic spatial-temporal dependencies. Additionally, it uses the k-shape clustering algorithm to calculate similar historical traffic patterns for each sample, thus simulating information propagation delays.
- OFA: A time series model based on LLM (Large Language Model). It processes time series data by segmenting it into patches and converting it into tokens for LLM processing. It

fine-tunes only the layer normalization and position encoding of LLM to retain its general capabilities.

- **STGLLM**: A spatial-temporal forecasting model based on LLM. It enhances LLM’s understanding of spatial-temporal data using time embedding and other external information, as well as prompts. It also fine-tunes only the layer normalization and position encoding of LLM.
- **BRITS**: A multivariate time series imputation model based on bidirectional RNNs (Recurrent Neural Networks). It employs a delayed error design for self-supervised training of the model. By using the consistency constraints of bidirectional RNNs, it addresses the error accumulation issue of unidirectional RNNs. It integrates both history-based and feature-based estimations.
- **E2GAN**: A multivariate time series imputation model based on GAN (Generative Adversarial Network). The generator uses an autoencoder structure, mapping incomplete inputs to a latent space with added random noise, and then gradually decoding them into complete sequences. Both the encoding and decoding modules of the generator and the discriminator use GRUI (Gated Recurrent Unit for data Imputation), a GRU that incorporates a time decay factor.
- **mTAN**: A multivariate time series imputation model based on VAE (Variational Autoencoder) and attention. It maps irregularly sampled sequences into a latent space using attention. It samples latent states from the latent space and then uses attention and RNN to obtain the complete sequence.
- **PriSTI**: A spatial-temporal data imputation model based on Diffusion Model and attention. It transforms the imputation problem into a generation problem by filling missing parts with random noise and then using the denoising module of the diffusion model to convert the noise into real values. It designs a conditional feature extraction module to provide a coarse-grained spatial-temporal dependency context prior for the spatial-temporal attention mechanism in the denoising module, thus enabling more accurate imputation.

C.2 Datasets

The detail of four dataset used in our experiments are summarized in Table 6. Data is sampled every 30 seconds and compiled into 5-minute intervals. The table reveals that the datasets contain a small number of edges, indicating that all four have comparatively sparse graph structures.

Table 6: Datasets

Datasets	Samples	Nodes	Edges	Interval	Time Range
PEMS03	26208	358	547	5min	09/01/2018-11/30/2018
PEMS04	16992	307	340	5min	01/01/2018-02/28/2018
PEMS07	28224	883	866	5min	05/01/2017-08/31/2017
PEMS08	17856	170	295	5min	07/01/2016-08/31/2016

C.3 Missing Patterns

We construct missing data on the complete dataset to train and test the model’s imputation capabilities. The experiment is designed with two different types of missing data patterns, namely random missing(RM) and spatial-temporal continuous missing(CM), which are defined as follows: **RM**: A missing pattern that is unrelated to both time and space, and is entirely random. In constructing this pattern, it is only necessary to randomly mask a portion of the data according to the missing rate. **CM**: A pattern of missingness that has a strong correlation with both time and space, characterized by simultaneous missing data in a specific area over a certain period. We define three consecutive time steps as one patch and use graph clustering algorithms to divide the graph into several smaller regions. When constructing the missing data, we randomly select patches and small regions, masking all the data within them.

C.4 Model Configurations

The hyperparameters used in our model for all experiments are the same, as summarized in Table 7:

Table 7: MODEL CONFIGURATIONS.

Module	Hyper Parameters	Note	Value
Spatial-Temporal embedding	d_t	the dimension of time embedding	16
	d_n	the dimension of topology-aware node embedding	16
	K	the number of truncated eigenvectors	16
Spatial-Temporal Tokenizer	d_T	the dimension of Temporal Tokenizer	64
Hypergraph Learning	M	the number of region-level tokens	128
	d_H	the dimension of hidden space in Hypergraph	128
LLM	d_{LLM}	the dimension of the word embeddings in LLM	768
	Layers	the number of LLM layers utilized	3

C.5 Parameter Efficacy

An important question to consider is whether the LLM significantly increases the computation cost. We have summarized the computation cost of main baselines and STD-LLM in Table 8. It can be observed from the table that, although our model has a large number of parameters, only 2.69% of them require training, and our model also has the fastest inference speed. The incorporation of LLM does indeed substantially increase the number of parameters, which leads to higher GPU memory usage. However, thanks to the relatively simple structure of LLM, all operations can be highly parallelized, thus not significantly impacting the training and inference time. Additionally, the regional-level tokens constructed by our hypergraph module also reduce the number of tokens, thereby enhancing computation speed.

Table 8: The computation cost on the PEMS08 with the batchsize=64.

Method	Parameters	Trainable Parameters	Trainable Ratio(%)	Interface Time(s/epoch)
PriSTI	937646	931246	99.31	2193.27
PDFormer	537565	531165	98.80	9.49
STGLLM	64014315	1016808	1.58	8.36
STD-LLM (ours)	64754907	1746520	2.69	5.53

Additionally, we have further tested the impact of the hypergraph module on the model’s inference efficiency. The results of the experiments are summarized in Table 9, we record the time cost to infer the entire test set (in seconds).

Table 9: Comparison of inference times with the batchsize=64.

Method	PEMS03	PEMS04	PEMS07	PEMS08
w hypergraph	9.27	6.23	12.33	5.53
w/o hypergraph	19.973	11.50	55.32	7.31

From the results, we can observe that the hypergraph module significantly enhances the efficiency of the model, particularly on large graph structures. On the PEMS07 dataset with 883 nodes, the hypergraph module can improve inference efficiency by nearly five times.

D Error Bars

All experiments were conducted three times, and the final metrics were taken as the average of the three trials. We present the standard deviations for STD-LLM in the forecasting and imputation experiments in Table 10 and Table 11.

Table 10: Standard deviations of STD-LLM in the forecasting experiment.

Metric	PEMS03	PEMS04	PEMS07	PEMS08
MAE	14.89 ± 0.0636	18.31 ± 0.0321	19.71 ± 0.1153	13.85 ± 0.0011
RMSE	25.38 ± 0.3181	30.32 ± 0.0458	32.99 ± 0.1374	23.43 ± 0.1123
MAPE(%)	15.63 ± 0.2616	11.96 ± 0.0251	8.32 ± 0.0611	9.01 ± 0.0230

Table 11: Standard deviations of STD-LLM in the imputation experiment on PEMS08.

Metric	RM 30%	RM 70%	CM 30%	CM 70%
MAE	12.14 ± 0.0321	14.38 ± 0.0871	19.36 ± 0.1352	22.18 ± 0.0793
RMSE	19.44 ± 0.0400	22.92 ± 0.0700	34.53 ± 0.2150	39.26 ± 0.4179
MAPE(%)	8.06 ± 0.0360	9.46 ± 0.1014	12.30 ± 0.0642	13.56 ± 0.1212

E Detailed Definition for Constraint Loss

We decompose the constrain loss \mathcal{L}_C in Equation 9 into \mathcal{L}_G and \mathcal{L}_R :

$$\begin{aligned}\mathcal{L}_G &= - \sum_{m=1}^M \sum_{i,j(i \neq j)} S_{m,i} S_{m,j} A_{i,j}, \\ \mathcal{L}_R &= \log \pi(\text{Softmax}(\sum_{m=1}^M S_{m,:}) | \alpha),\end{aligned}\tag{11}$$

Firstly, as the attention score, $S_{m,:}$ satisfies the properties: $\sum_{i=1}^N S_{m,i} = 1$. It is clear that the more edges there are, the smaller the minimum value of \mathcal{L}_G can be. Consider a complete graph of size P , where:

$$\begin{aligned}\mathcal{L}_G &= - \sum_{m=1}^M \sum_{i,j(i \neq j)} S_{m,i} S_{m,j}, \\ &= - \sum_{m=1}^M \sum_i S_{m,i} (1 - S_{m,i}) = -M + \|S \odot S\|_1.\end{aligned}\tag{12}$$

\odot means Hadamard Product. It is clear that the way to minimize \mathcal{L}_G is to distribute the S evenly, that is, $S_{m,i} = \frac{1}{P}$, at which point $\mathcal{L}_G = -\frac{M(P-1)}{P}$. When we shift our focus to a regular graph of size N , the smaller the \mathcal{L}_G , the more readily the hypergraph module can focus attention on larger complete subgraphs or subgraphs with stronger connectivity, thereby integrating the graph structure into the model. Of course, the premise of doing this is that the graph we are dealing with is a relatively sparse graph, containing many small complete subgraphs or subgraphs with strong connectivity. Otherwise, the hypergraph module might focus attention only on a few large complete subgraphs. If the graph we are facing is composed of just a few large complete subgraphs, then it is possible to achieve better results using prior knowledge.

Regarding \mathcal{L}_G , we intend for it to serve a guiding role during the training process and do not wish for the model to excessively reduce \mathcal{L}_G . Doing so could very likely lead to overfitting, which might result in extremely low attention being allocated to some nodes. Therefore, we introduce a regularization term \mathcal{L}_R . \mathcal{L}_R is based on the Dirichlet distribution π , which is defined as follows:

$$\begin{aligned}
\Theta &= \{\theta_1, \theta_2, \dots, \theta_N\}, \sum_i^N \theta_i = 1, \\
\alpha &= \{a_1, a_2, \dots, a_N\}, \\
\pi(\Theta|\alpha) &= \frac{\Gamma(\sum_i a_i)}{\prod_i \theta_i^{a_i-1}}.
\end{aligned} \tag{13}$$

The expected value of the Dirichlet distribution $E(\theta_i) = \frac{a_i}{\sum_i a_i}$. Thus, we can set $\alpha = \{1.05\}^N$ (a small value greater than 1), which constrains the hypergraph module to aggregate each node equally. In practice, we believe that nodes of greater significance should receive more attention. Therefore, we incorporate the degree of the nodes: $\alpha = \{1.05\}^N + c \times \text{Softmax}(\text{diag}(D))$. Here, *diag* refers to the operation of extracting the diagonal elements of a matrix, and c is a coefficient.

F Few-shot Performance on Pre-trained STD-LLM

In Section 4.4, we verified that the STD-LLM, which had not been pre-trained on spatial-temporal data, also possesses strong few-shot performance. So, would an STD-LLM that has been pre-trained on a specific spatial-temporal dataset exhibit even stronger few-shot performance? Can a pre-trained STD-LLM play a positive role in the training on other spatial-temporal datasets? To this end, we conduct some experiments to verify. We tested the few-shot performance and full dataset training performance of the STD-LLM pre-trained on PEMS07 for the PEMS08 and PEMS04 datasets, with the results summarized in Table 12.

Table 12: Few-shot on pre-trained STD-LLM.

Ratio	PEMS04			PEMS08		
	MAE	RMSE	MAPE(%)	MAE	RMSE	MAPE(%)
5%	22.11	35.24	14.76	17.05	27.16	10.92
10%	21.03	33.71	13.75	17.10	27.41	10.83
20%	20.21	32.99	13.18	16.01	26.12	10.56
100%	18.20	30.13	11.94	13.77	23.52	8.98

The results indicate that the few-shot performance of the pre-trained STD-LLM has seen a significant enhancement, achieving comparable performance to that of the non-pre-trained model using 20% of the data with just 5% of the data. Additionally, the performance of the model trained on the full dataset has also improved, demonstrating that STD-LLM can correctly transfer the knowledge acquired from pre-training to new tasks.

G Visualization

We have plotted some results for forecasting and imputation. It can be observed that STD-LLM can accurately follow the trend of data changes and also make corresponding adjustments to sudden changes in the data.

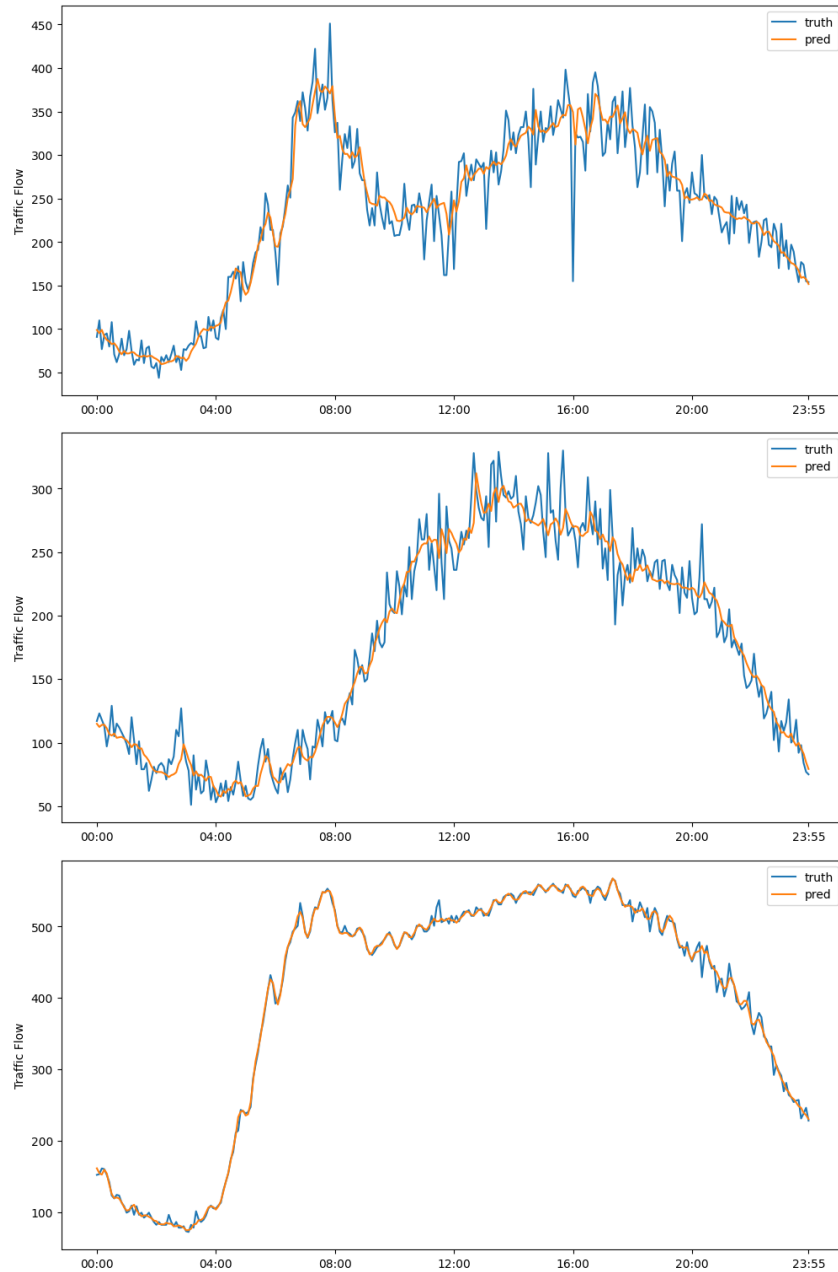


Figure 4: Traffic flow forecasting.

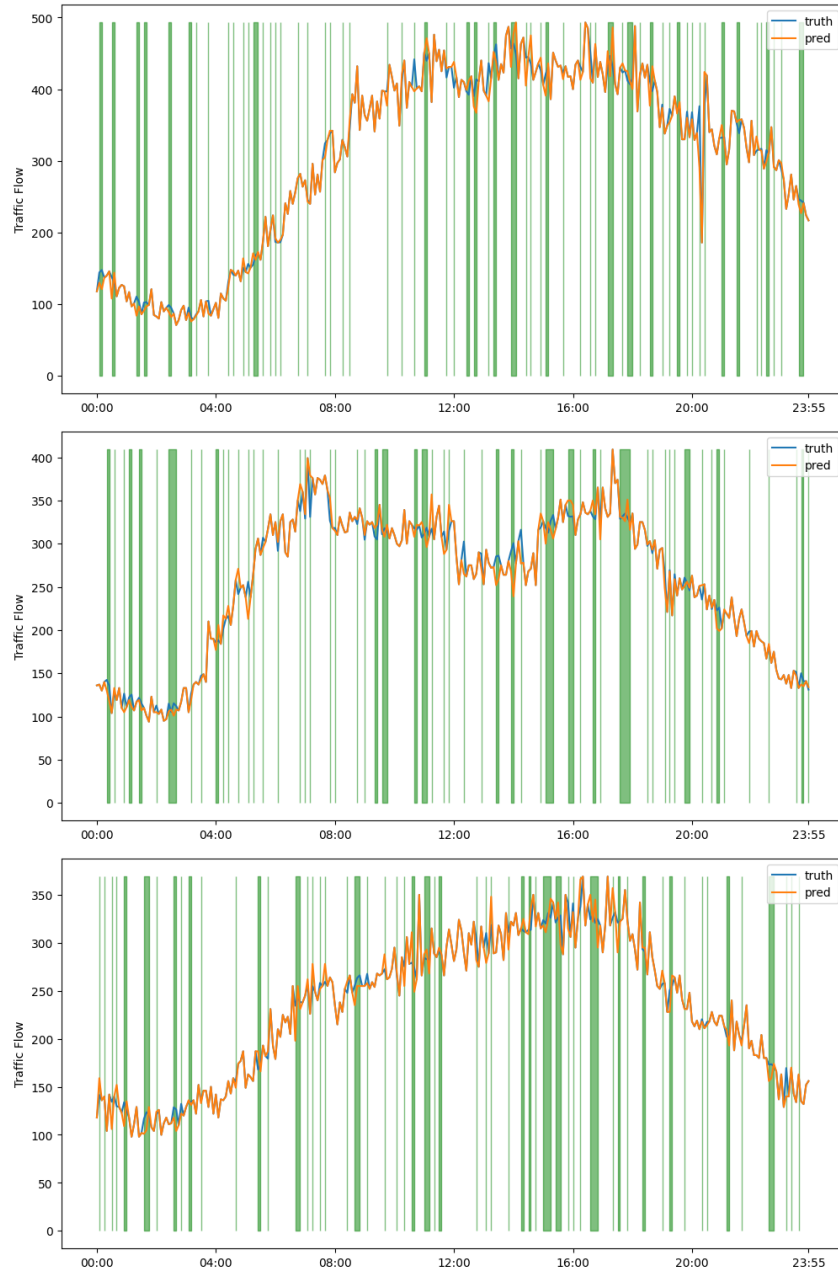


Figure 5: Traffic flow imputation. The green areas indicate the locations where data is missing and requires imputation.